Scanning Electrochemical Microscopy: Theory and Application of the Transient (Chronoamperometric) SECM Response

ARTICLE *in* ANALYTICAL CHEMISTRY · AUGUST 1991

Impact Factor: 5.64 · DOI: 10.1021/ac00013a019 · Source: PubMed

5 AUTHORS, INCLUDING:

Bright Dornblaser
Texas Commission on Environmental Quality
9 PUBLICATIONS **200** CITATIONS
SEE PROFILE

Laurette S. Tuckerman
MINES ParisTech
104 PUBLICATIONS **2,577** CITATIONS
SEE PROFILE

Scanning Electrochemical Microscopy: Theory and Application of the Transient (Chronoamperometric) SECM Response

Allen J. Bard,* Guy Denuault, and Richard A. Friesner[1]

Department of Chemistry, The University of Texas at Austin, Austin, Texas 78712

Bright C. Dornblaser

Center for Non Linear Dynamics, Department of Physics, The University of Texas at Austin, Austin, Texas 78712

Laurette S. Tuckerman

Department of Mathematics, The University of Texas at Austin, Austin, Texas 78712

A study of the transient (chronoamperometric) response of the scanning electrochemical microscope (SECM) is presented. SECM transients were simulated digitally with a novel integrator based on a Krylov algorithm. The transients observed with planar electrodes (PE), microdisks (MD), and thin-layer cells (TLC) are shown to be limiting cases that fit the simulated SECM transients at very short, intermediate, and long times, respectively. A procedure is established that, provided the tip radius is known, allows the determination of the diffusion coefficient of the species in solution independent of its concentration and the number of electrons transferred in the electrode reaction. Experimental SECM transients are reported for the electrochemical oxidation of $Fe(CN)_6^{4-}$ in KCl; the diffusion coefficient of $Fe(CN)_6^{4-}$ was found to agree very well with the literature value.

INTRODUCTION

Previous papers have described the theory (*1-3*) and applications (*4-12*) of the scanning electrochemical microscope (SECM) operating in the steady-state current regime. The tip current, due to an electrochemical reaction at the tip (e.g., $O + ne \rightarrow R$), is perturbed by the presence of the substrate, which can be an electronic insulator or a conductor. For an insulator, the substrate blocks diffusion of O to the tip ("negative feedback"). With a conductive substrate, if it is biased by an external source or by a solution redox species to a potential where oxidation of R to O occurs, the flux of O to the tip is increased ("positive feedback"). The substrate will affect the tip current when the tip-to-substrate distance, d, is within a few tip radii, a. The steady-state tip current, which can be calculated from the steady-state concentration profiles in the gap between the microdisk tip and the substrate, provides information about the topography (*2, 10, 13*), as well as the chemical and electrochemical reactivity (*2, 11, 13*) of the substrate surface. In this paper we consider the transient SECM response, i.e., the microdisk current, i_T, as a function of time, t, which has not been considered in previous work. For example, the i-t response provides a measure of the rate of establishment of the steady state and the maximum rate at which SECM topographic scans can be made. Moreover, the transient (chronoamperometric) response is related to the rates of diffusion and of any homogeneous chemical reactions in solution, as well as the topography and the rate of electron transfer on both electrodes. Because the SECM involves small microdisk tip diameters, $2a$, typically 0.6-25 μm, and very small tip-to-substrate distances (e.g., $d \leq 2a$), the effective mass-transfer coefficient in the gap region is very high. It should thus be possible to study very high rates of diffusion or very fast homogeneous chemical reactions by transient SECM methods. This paper deals with the theory of the transient SECM response in the absence of homogeneous and heterogeneous kinetic complications. Since the geometry of the SECM does not allow one to derive a closed-form analytical solution for the current, a two-dimensional numerical simulation of the diffusion between the tip and the substrate was used to generate the transient response as a function of tip-substrate distance. We compare the simulated chronoamperometric response of the SECM with approximations based on known electrode geometries and show that the tip currently successively follows the time response of a planar electrode, a microdisk, and a thin-layer cell. These electrode geometries yield closed-form analytical solutions that provide a good guide for the prediction of the SECM chronoamperometric response.

We show that an analysis of the SECM transient yields a critical time, t_c, when the tip current senses the presence and nature of the substrate. A working curve of the critical time as a function of d is presented. We show that measurement of t_c from the transient and of d from the steady-state curve of $i_T/i_{T,\infty}$ (*1*) allows the determination of D, without knowledge of n or C^*. In this treatment, $i_{T,\infty}$ is the steady-state tip current when the tip is far from the substrate and is given by $i_{T,\infty} = 4nFDC^*a$; n is the number of electrons in the tip electrode reaction, F is the Faraday constant, C^* is the concentration, D is the diffusion coefficient, and a is the microdisk radius. If D is known, a measurement of t_c also allows the absolute determination of the tip-substrate distance independent of the working curve (*1*) $i_T/i_{T,\infty} = f(d)$. Finally, experimental SECM transients are reported for the oxidation of $Fe(CN)_6^{4-}$ in KCl solution and these are compared to the theoretical curves.

EXPERIMENTAL SECTION

Reagents. Solutions of 50 mM $K_4Fe(CN)_6 \cdot 3H_2O$ (MCB Manufacturing Chemists Inc., Cincinnati, OH) and 1 M KCl (Baker Analyzed, J. T. Baker Inc., Phillipsburg, NJ) were prepared with deionized water (Milli-Q, Millipore Corp.).

Electrodes. The SECM tip was a 25 μm diameter Pt microdisk encased in glass; its construction followed the procedure reported previously (*2*). The glass surrounding the Pt was polished into a conical shape and the bottom polished flat to yield a Pt disk with glass insulation with a radius about 24 times bigger than the Pt disk. Before each experiment, the tip was polished on a Nylon cloth with 0.25-μm diamond paste (both from Buehler Ltd., Lake Bluff, IL). The reference electrode was a saturated calomel electrode (SCE). The substrate used throughout was a glass disk

* To whom correspondence should be addressed.
[1] Present address: Department of Chemistry, Columbia University, New York, NY 10027.

0003-2700/91/0363-1282$02.50/0

with gold (about 800 Å thick) sputtered on half of the disk. This substrate offered both insulating and conducting areas.

Apparatus. The SECM apparatus has been described previously (*4, 5*). The cell was mounted on an X-Y stage controlled by piezoelectric drivers (inchworms 100 Å/s to 2 mm/s, Burleigh Instruments, Fischer, NY), and the tip position was controlled by a similar Z piezoelectric inchworm. The SECM setup was placed on an air table (NRC pneumatic isolation mount, Newport Corp., Fountain Valley, CA) and shielded with a Faraday cage. A two-electrode configuration was employed, with the tip potential controlled by a Princeton Applied Research PAR Model 175 programmer, and the tip current was monitored by a home-built current follower with a rise time of about 100 μs. The SECM chronoamperometric response was recorded with a Norland Model 3001A/DMX digital processing oscilloscope (Norland Corp., Fort Atkinson, WI).

Procedure. After a potential step from +0.1 to +0.5 V vs SCE, the tip current was recorded as a function of time for different tip to substrate distances above the conducting (gold) substrate or insulating (glass) substrate. The conducting substrate was unbiased, with its potential controlled by the local ratio of the concentration of oxidized and reduced species.

THEORY

We first present analytical approximations that describe the chronoamperometric response of the SECM when the tip potential is stepped from a value where no electrochemical reaction occurs to one where a reduction or oxidation takes place at a diffusion-controlled rate. These expressions have been established previously for different electrode geometries and are approximately valid for different time windows of the SECM i–t curve. They are particularly useful in providing a physical feeling for the SECM transient behavior in different time regimes.

It is convenient to use Dt/a^2 as the dimensionless time, where a^2/D is a measure of the time taken by the species to diffuse over a distance a equal to the tip radius. We also normalize all distances with respect to a. As is common practice in SECM theory, we normalize the tip current with respect to the steady-state tip current at infinity, $i_{T,\infty}$.

(a) At very short times, the thickness of the diffusion layer is small with respect to a and semiinfinite linear diffusion applies. Under these conditions, the Cottrell equation (*14*) holds. Normalization with respect to $i_{T,\infty}$ yields

$$\frac{i_{PE}}{i_{T,\infty}} = \frac{\pi^{1/2}}{4}\left(\frac{Dt}{a^2}\right)^{-1/2} \qquad Dt/a^2 \ll 1 \qquad (1)$$

where i_{PE} is the chronoamperometric response of a planar electrode (the Cottrell equation).

(b) At short times, when the diffusion layer is still small with respect to d but microdisk edge effects become important, the tip behaves as a microdisk; a quasi hemispherical diffusion field is established, and the transient deviates from the Cottrell i–t curve. The current then follows the chronoamperometric response of a microdisk, e.g., as given by Shoup and Szabo (*15*). Normalization of their expression with respect to $i_{T,\infty}$ leads to

$$\frac{i_{MD}}{i_{T,\infty}} = 0.7854 + \frac{0.8862}{2}\left(\frac{Dt}{a^2}\right)^{-1/2} + 0.2146\exp\left[-\frac{0.7823}{2}\left(\frac{Dt}{a^2}\right)^{-1/2}\right] \qquad (2)$$

where i_{MD} is the chronoamperometric response of a microdisk. At long times, in the absence of substrate effects, the steady-state current to a microdisk would be established and under these conditions eq 2 would yield $i_{MD}/i_{T,\infty} = 1$.

(c) At intermediate and long times, the substrate interacts with the diffusion field, i.e., $(Dt)^{1/2} > d$, and it is convenient to draw a parallel between the tip–substrate system and a thin-layer cell (TLC) (*2*). Two cases need to be considered depending on the type of substrate.

(1) For a conducting substrate, where the reaction at the substrate is the reverse of the tip reaction and occurs at a mass-transfer-controlled rate, we take the chronoamperometric response of a TLC (a four-electrode system), where the cavity is bounded by two electrodes, one acting as an anode, the other as a cathode (with the cell also containing a counter and a reference electrode). The current at the cathode has been derived (see eq 87 of ref *16*); normalization of this expression with respect to $i_{T,\infty}$ leads to

$$\frac{i_{TLC}}{i_{T,\infty}} = \frac{\pi}{4(d/a)}\left[1 + 2\sum_{n=1}^{\infty}\exp\left(-\frac{n^2\pi^2}{(d/a)^2}\frac{Dt}{a^2}\right)\right] \qquad (3)$$

where d is the distance between the tip and the substrate. At long times, the TLC current reaches a steady state and eq 3 yields the expression suggested in ref 2, $i_{TLC}/i_{T,\infty} = (\pi/4)(a/d)$.

(2) For an insulating substrate, we take the chronoamperometric response of a TLC where the cavity is bounded by one electrode and an insulating wall. The analytical expression for the concentration profiles within such a cell has been derived (see eq 4 of ref *17*). Differentiation to obtain the current at the electrode and normalization with respect to $i_{T,\infty}$ leads to

$$\frac{i_{TLC}}{i_{T,\infty}} = \frac{\pi}{2(d/a)}\sum_{n=0}^{\infty}\exp\left[-\frac{(2n+1)^2\pi^2}{4(d/a)^2}\frac{Dt}{a^2}\right] \qquad (4)$$

At long times, depletion of the species within the TLC leads to zero current and eq 4 yields $i_{TLC}/i_{T,\infty} = 0$. In the SECM, the current decays to a steady state, non-zero value, because electroactive material continues to diffuse to the tip from the space between the edges of the insulator surrounding the microdisk and the substrate. The SECM in this regime can thus be thought of as a "leaky" TLC.

Table I illustrates the chronoamperometric response given by eqs 1–4 from very short to very long times. Equations 3 and 4, valid for a TLC at long times, become unwieldy at shorter times and are no longer useful as the limit Dt/a^2 approaches 0. When $Dt/a^2 > (d/a)^2$, the relative current reaches a steady state for a two-electrode TLC and decays to 0 for a one-electrode TLC. In other words, for $t \geq d^2/D$, the species have diffused across the gap of distance d and now probe the presence and nature of the substrate. For a conducting substrate, the species that were oxidized or reduced on the tip are regenerated and a steady-state concentration profile is rapidly established. For an insulating substrate, however, rapid depletion of the species leads to a 0 current. Table I also shows that for $t \ll d^2/D$, the SECM tip current should follow the chronoamperometric response of a PE; it then rapidly deviates to that of a MD. When $t \geq d^2/D$, the SECM tip current should follow the response of a TLC.

Equations 1–4 are adequate for a semiquantitative understanding of the SECM i–t curve. However, since an exact solution to the differential equations governing the concentration distribution between the tip and the substrate is, to our knowledge, not known, accurate prediction of the SECM time response requires a digital simulation.

NUMERICAL SIMULATION

The fundamental diffusion equations for the SECM geometry and the boundary conditions have been given in a previous treatment of the steady-state current (*1*). Modeling the SECM places two conflicting demands on a numerical simulation. A high spatial resolution is necessary at both the substrate and electrode surfaces, where the electrochemical reactions occur; however, the diffusion between substrate and

Table I. Approximate SECM Transients Based on the Chronoamperometric Response for a Planar Electrode (Second Column), a Microdisk (Third Column), a Thin-Layer Cell with Two Electrodes (Fourth to Sixth Columns), and a Thin-Layer Cell with One Electrode (Seventh to Ninth Columns)[a]

			$i_{TLC}/i_{T,\infty}$					
			conducting substrate eq 3			insulating substrate eq 4		
Dt/a^2	$i_{PE}/i_{T,\infty}$ eq 1	$i_{MD}/i_{T,\infty}$ eq 2	$d/a = 0.1$	$d/a = 1$	$d/a = 10$	$d/a = 0.1$	$d/a = 1$	$d/a = 10$
10^{-5}	140.125	140.906	140.125			140.125		
10^{-4}	44.311	45.095	44.311	44.311		44.311	44.311	
10^{-3}	14.012	14.797	14.014	14.012		14.011	14.012	
10^{-2}	4.431	5.221	7.855	4.431	4.431	1.332	4.431	4.431
10^{-1}	1.401	2.249	7.854	1.401	1.401	0.000	1.401	1.401
1	0.443	1.374	7.854	0.785	0.443	0.000	0.133	0.443
10^{1}	0.140	1.115	7.854	0.785	0.140	0.000	0.000	0.140
10^{2}	0.044	1.036	7.854	0.785	0.079	0.000	0.000	0.013
10^{3}	0.014	1.011	7.854	0.785	0.079	0.000	0.000	0.000
10^{4}	0.004	1.004	7.854	0.785	0.079	0.000	0.000	0.000
10^{5}	0.001	1.001	7.854	0.785	0.079	0.000	0.000	0.000

[a] The TLC expressions, eqs 3 and 4, were computed with 100 terms in the series.

electrode takes place over a distance several orders of magnitude greater. A uniform grid of both high resolution and large extent is prohibitively expensive (*1*). The use of several exponential grids within the domain, as used in the previous simulation (*1*) of the steady-state behavior of the SECM, reconciles these two demands. A simulation of the time evolution of the SECM and its transient behavior can be treated as a large set of coupled, ordinary differential equations (*18*, *19*). These equations are stiff because of the different length scales on the exponential grids.

Modeling of the SECM transient assumes the oxidation reaction, $R - ne \rightarrow O$, occurs at the electrode tip. The concentrations of the two species, $C_O(r,z)$ and $C_R(r,z)$, can be represented by the second-order partial differential equations for diffusion to a disk:

$$\frac{\partial C_O(r,z)}{\partial t} = D_O\left[\frac{\partial^2 C_O(r,z)}{\partial r^2} + \frac{1}{r}\frac{\partial C_O(r,z)}{\partial r} + \frac{\partial^2 C_O(r,z)}{\partial x^2}\right] \quad (5)$$

$$\frac{\partial C_R(r,z)}{\partial t} = D_R\left[\frac{\partial^2 C_R(r,z)}{\partial r^2} + \frac{1}{r}\frac{\partial C_R(r,z)}{\partial r} + \frac{\partial^2 C_R(r,z)}{\partial z^2}\right] \quad (6)$$

The scaling of variables and choice of boundary conditions exactly followed the previous SECM simulations (*1*). If one chooses as an initial condition ($t = 0$) that $C_O(r,z) = C_O^*(r,z)$ (the oxidized bulk concentration) and assumes that the diffusion coefficients for both species are equal, $D_O = D_R$, then eqs 5 and 6 can be replaced with a single equation for the scaled oxidized species, $X(r,z) = C_O(r,z)/C_O^*(r,z)$. The concentration of the reduced species is then $1 - [C_O(r,z)/C_O^*(r,z)]$. The boundary conditions described in ref 1 now apply to a domain for one scaled concentration, and with lengths scaled by the tip radius, a. Along the tip electrode surface, $z = 0$, the assumption of fast kinetics gives a homogeneous boundary condition, $X(r,0) = 0$. There is a nonhomogeneous boundary condition $X(r,d/a) = 1$ on a conducting substrate, at a distance $z = d/a$ from the electrode, for the same reason. As usual, along the glass electrode sheath surrounding the tip and on an insulating substrate, there is a no-flux (Neumann) boundary condition, and we assume that the bulk concentration is regained at the radius of the glass sheath, RG. The resulting diffusion equation in the single variable $X(r,z)$ with these mixed inhomogeneous boundary conditions is not known to have an analytical solution. We write our single-differential equation as a set of ordinary differential equations, as discussed previously (*18*, *19*), of a form that can be solved by a matrix approach.

$$d\mathbf{x}/dt = A_r\mathbf{x} + A_z\mathbf{x} + \mathbf{b} \quad (7)$$

$$(A_r x)(r_i,z_j) = \alpha_i^r x(r_{i-1},z_j) + \beta_i^r x(r_i,z_j) + \gamma_i^r x(r_{i+1},z_j) \quad (8)$$

$$(A_z x)(r_i,z_j) = \alpha_j^z x(r_i,z_{j-1}) + \beta_j^z x(r_i,z_j) + \gamma_j^z x(r_i,z_{j+1}) \quad (9)$$

where α, β, and γ are coefficients of the Laplacian in cylindrical coordinates and $A_r x(r_i,z_j)$ and $A_z x(r_i,z_j)$ represent an element of the matrix–vector product at point i,j. Since we used the exponential grids described in ref 1, these coefficients take a more complicated form than those in the equally spaced finite difference formula. Vector $\mathbf{b}$ incorporates the effect of the inhomogeneous boundary condition on the neighboring points.

Instead of the Lanczos approach (*18*, *19*), a new algorithm for the solution of large sets of stiff ordinary differential equations based upon exact propagation in a small Krylov space (*20*) was used. Details of this approach are given elsewhere (*20*, *21*), and only an outline of the method will be given here. The exact solution to eq 7 is

$$\mathbf{x}(t) = \mathbf{x}_0 + \frac{e^{\mathbf{A}t} - \mathbf{I}}{\mathbf{A}}(\mathbf{A}\mathbf{x}_0 + \mathbf{b}) \quad (10)$$

where $\mathbf{A} = \mathbf{A}_r + \mathbf{A}_z$. This operation is carried out in a reduced subspace as follows. As described in ref 20, a Krylov space is formed by successive action of the Jacobian $\mathbf{A}$ on the vector $(\mathbf{A}\mathbf{x}_0 + \mathbf{b})$, i.e., the first vector $\Psi^1 = (\mathbf{A}\mathbf{x}_0 + \mathbf{b})$ and Ψ^k result from orthonormalizing $\mathbf{A}\Psi^{k-1}$ to all previous Ψ's. Thus K iterations yield K Krylov vectors; for this work, 15 Krylov vectors were used to span the 15 dimensional Krylov subspace. The N by K matrix Ψ is defined as $\Psi_{ik} = \Psi_i^k$. Multiplication of a Krylov vector by Ψ takes the components of the vector from the Krylov space back to R^n, and $\Psi^\dagger$ projects a vector in R^n into the Krylov subspace. While orthonormalizing the vectors Ψ^k one can construct a matrix

$$\tilde{\mathbf{A}}_{kl} = \langle \Psi^k | \mathbf{A} | \Psi^l \rangle \quad (11)$$

$\tilde{\mathbf{A}}$ is a K by K upper Hessenberg matrix and can be diagonalized by the QR algorithm so that

$$\tilde{\mathbf{A}} = \mathbf{U}\Lambda\mathbf{U}^{-1} \quad (12)$$

where $\mathbf{U}$ is the matrix of eigenvalues and Λ is the diagonal matrix of eigenvalues of $\tilde{\mathbf{A}}$.

Most numerical methods approximate the exact solution to this linear problem by approximating the exponential of $\mathbf{A}$. The exponential is treated as a polynomial expansion in explicit methods or by rational approximations in implicit

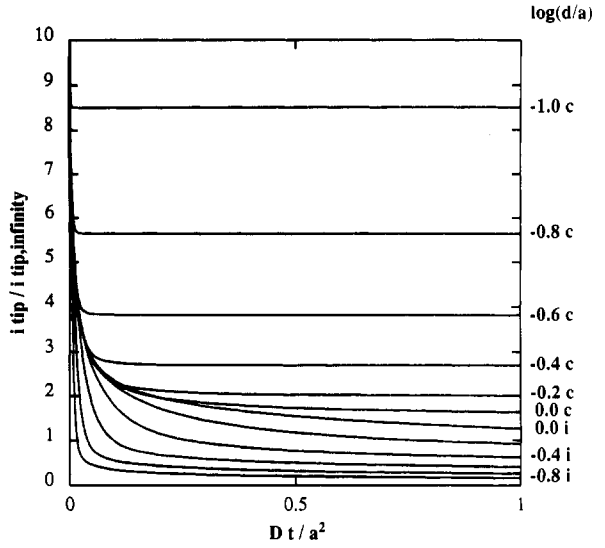

Figure 1. Simulated SECM transients. The top curves correspond to a conducting substrate (log (d/a) = −1, −0.8, −0.6, ..., 0 from the top downward); bottom curves correspond to an insulating substrate (log (d/a) = −1, −0.8, −0.6, ..., 0 from the bottom upward). These results were obtained for an RG (insulating sheath radius/tip radius) of 10 and on the assumption that oxidized and reduced species had the same diffusion coefficient.

schemes. In both cases the exact matrix **A** is used. In the method described here, exponential propagation involves the exact exponential of the approximate matrix $\tilde{\mathbf{A}}$. Our solution is obtained as

$$\mathbf{x}(t) = \mathbf{x}_0 + \Psi\mathbf{U}\frac{e^{\Lambda t} - \mathbf{I}}{\Lambda}\mathbf{U}^{-1}\Psi^{\dagger}(\mathbf{A}\mathbf{x}_0 + \mathbf{b}) \qquad (13)$$

where the notation $(e^{\Lambda t} - \mathbf{I})/\Lambda$ is shorthand for diag$[(e^{\Lambda_i t} - 1)/\Lambda_i]$.

The concentrations of the reduced species are integrated to some specified time, to obtain concentration profiles. This procedure was carried out for different spacings, d, for both conductive and insulating substrates. The current was then calculated by a summation of the fluxes at the tip electrode surface.

The calculation of SECM transient and steady-state currents presented here can also be accomplished by other methods. For example, we recently treated this problem, with inclusion of a homogeneous reaction in the solution between tip and substrate, by the alternating direction implicit (ADI) method (22). The normalized current–time–distance curves found by the ADI calculations were in excellent agreement with those reported here. Moreover, the ADI method was more efficient for these calculations, which involved solving two tridiagonal matrix equations when the cylindrical Laplacian separates into two directions. However, the Krylov integrator approach may have advantages in other problems.

RESULTS AND DISCUSSION

Figure 1 shows simulated transients in a dimensionless form ($i_T/i_{T,\infty} = f(Dt/a^2)$) for a conducting (C) and insulating (I) substrate for different values of d/a. From the top curve downward, log (d/a) = −1, −0.8, −0.6, ..., 0 for a conductor, and from the bottom curve upward, log (d/a) = −1, −0.8, −0.6, ..., 0 for an insulator. At long times, the simulated tip transients converge to the steady-state tip currents simulated previously (1). While i_T reaches a steady state very rapidly with a conducting substrate, it exhibits a quasi steady state with an insulator. With no feedback diffusion from the insulating substrate to the tip, depletion of species first occurs within the thin layer of solution bounded by the conductive (Pt) microdisk and the substrate. A true steady state is established

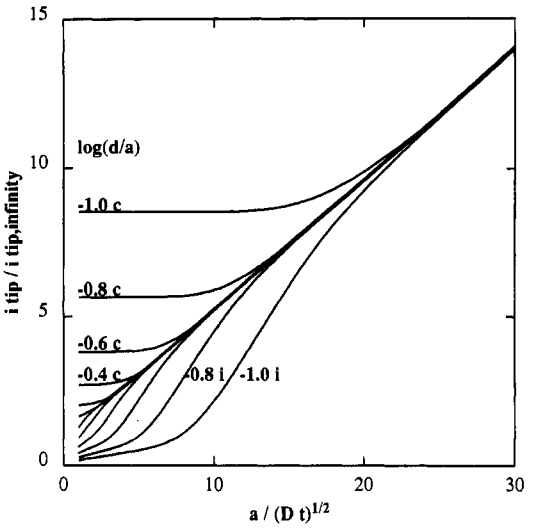

Figure 2. Same transients as in Figure 1, but plotted as a function of the inverse square root of the dimensionless time.

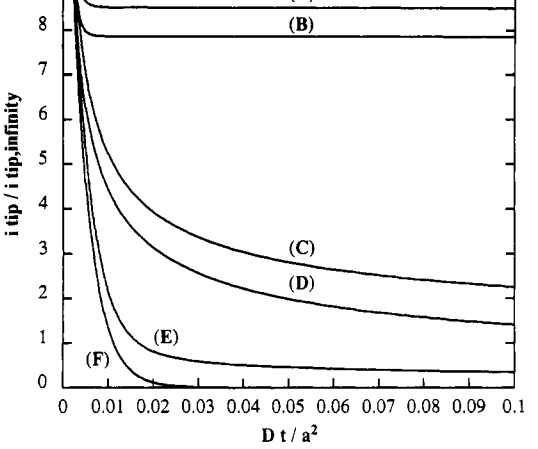

Figure 3. Comparison of simulated SECM transients in the form $i_T/i_{T,\infty} = f(Dt/a^2)$, with transients corresponding to different electrode geometries: (A) simulated SECM transient for a conducting substrate; (B) two-electrode TLC, eq 3; (C) MD, eq 2; (D) PE, eq 1; (E) simulated SECM transient for an insulating substrate; (F) one-electrode TLC, eq 4. Curves A, B, E, and F were computed with d/a = 0.1.

later, when depletion and a steady concentration profile exist all the way to the edge of the insulating sheath where it meets the bulk solution. Thus with insulating substrates, the rate of attainment of steady state depends on the thickness of the insulating region around the microdisk. All calculations here were carried out with a ratio of insulating sheath radius to disk radius, r, termed RG, of 10. Steady state at an insulating substrate would be reached more quickly with a smaller RG.

In Figure 2 the simulated tip currents are replotted as a function of the inverse square root of the dimensionless time in order to highlight the chronoamperometric response at very short times. Figures 3 and 4 illustrate a comparison between simulated transients and approximate analytical transients computed with eq 1–4. The simulated curves agree quite well with the MD approximation in the short time region (Figure 4) but show significant differences from the TLC approximation in the long time region (Figure 3), which does not account for leakage into the gap region for both conducting and insulating substrates. As expected, the shapes of the SECM transients follow closely the MD transients and rapidly deviate toward a constant $i_T > i_{T,\infty}$ for a conducting substrate and $i_T < i_{T,\infty}$ for an insulating substrate. Merger of the curves

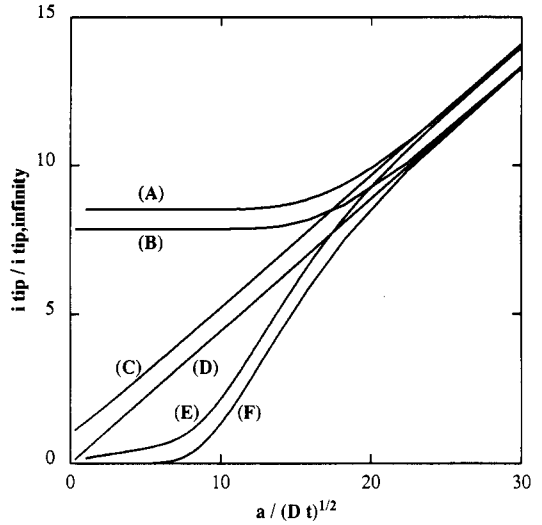

Figure 4. Same as in Figure 3, but in the form $i_T/i_{T,\infty} = f(a/(Dt)^{1/2})$.

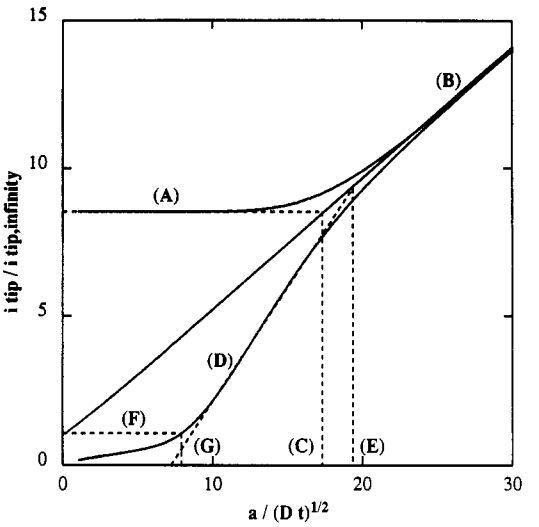

Figure 5. Plot of $i_T/i_{T,\infty}$ vs $a/(Dt)^{1/2}$ used for the evaluation of the dimensionless critical time: (A) horizontal line tangent to the steady-state simulated tip current for a conducting substrate; (B) line tangent to the short time simulated tip current; (C) dimensionless critical time for a conductor; (D) line tangent to the region of steepest gradient of a simulated tip current for an insulating substrate; (E) dimensionless critical time for an insulator (method 1); (F) horizontal line given by $i_T/i_{T,\infty} = 1$; (G) dimensionless critical time for an insulating substrate (method 2).

with the Cottrell equation occurs at times even shorter than those indicated in Figure 4.

From Figure 4 it is possible to distinguish two limiting SECM responses, a MD regime (short times) and a TLC regime (long times). We can define a time when the SECM undergoes a transition from the MD regime to the TLC regime—the critical time, t_c. Fundamentally, t_c is related to the time when the species diffuses to and from the tip probe in the presence of the substrate. Assume that a reduction takes place on the tip. For an insulating substrate, t_c is the time when the substrate first hinders the diffusion field of the oxidized species O. Thus t_c is of the order of d^2/D_O. However, for a conducting substrate, t_c is the time when the tip senses the increase in the local concentration of O (this increase is due to the diffusion of O from the bulk and from the substrate). In this case t_c is of the order of $d^2(1/D_R + 1/D_O)$ because it reflects the time taken by species R to diffuse from the tip to the substrate and that taken by species O to diffuse from the substrate to the tip. By assuming that $D_O = D_R = D$, t_c for a conducting substrate is about twice that for an insulating substrate. Indeed, both Figures 2 and 4 show that i_T (insulator) deviates from i_{MD} before i_T (conductor). The critical time, t_c, is therefore an important parameter that is directly related to the diffusion time of the species over the distance d. Since t_c is a function of d and D, measurement of t_c and d should allow direct determination of D; alternatively, measurement of t_c with a substrate of known D should lead to the tip–substrate distance, d.

In Figure 5 we show the procedure that was used to define an arbitrary dimensionless critical time. (The true critical time discussed above is not accessible directly from the transients.) The arbitrary defined values are easily obtained from a plot of $i_T/i_{T,\infty}$ vs $1/t^{1/2}$. For a conducting substrate, we take a simulated SECM transient and draw a horizontal straight line (A) at the level of the steady-state current. We then draw an oblique line (B) (which defines the transient behavior and is basically the analytical response of a MD) on the early part of the transient. The intersection of lines A and B leads to the dimensionless critical time Dt_c/a^2 (C). Two methods were used to define t_c with an insulating substrate. In method 1, a straight line (D) is drawn as a tangent to the region of steepest gradient. The intersection of lines B and D leads to Dt_c/a^2 (E). In method 2, for an insulating substrate, we can also define a t_c at an arbitrary value where the tip current is smaller than $i_{T,\infty}$. For example, t_c can be taken by drawing a horizontal straight line (F) for $i_T/i_{T,\infty} = 1$. The intersection of line F with the transient leads to the dimensionless critical time Dt_c/a^2 (G). By repeating these procedures for different values of d/a, we can construct working curves of $(Dt_c)^{1/2}/a$ as a function of d/a for conducting and insulating substrates (Figure 6). These curves can be used for the determination of D when d and a are known or for determination of d when D and a are known.

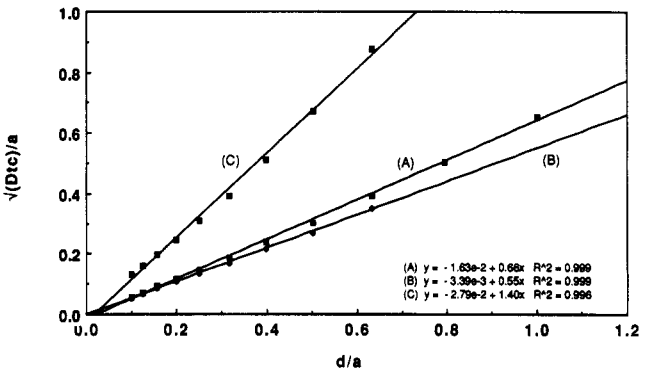

Figure 6. Plot of $(Dt_c)^{1/2}/a$ vs d/a used as a working curve for the determination of D when a conducting substrate (A) and an insulating substrate method 1 (B) and method 2 (C) are used. Plots are based on simulated SECM transients obtained for an RG of 10.

Again, one can get a feeling for this approach by considering a thin-layer cell. For a TLC, a critical time can be computed by equating the limiting current to the Cottrell transient current

$$nFADC^*/d = nFAD^{1/2}C^*/\pi^{1/2}t_c^{1/2} \quad (14)$$

Equation 14 yields the analytical working curve

$$(Dt_c)^{1/2} = d\pi^{-1/2} \quad (15)$$

As described previously, t_c can be evaluated from a plot of i_{TLC} against $1/t^{1/2}$. This equation is rigorous for a TLC. If d is known, eq 15 and the value of t_c yield a value of D independent of n and C^*. Alternatively, if D is known, eq 15 and the value of t_c yield the value of d for a TLC.

For the SECM situation, the relevant approximate equation is obtained by dividing eq 15 by a to yield

$$(Dt_c)^{1/2}/a = (d/a)\pi^{-1/2} \quad (16)$$

Table II. Experimental Results of SECM Transients with a Gold Substrate (a) and a Glass Substrate (b)[a]

(a) Gold

$i_T/i_{T,\infty}$	d/a	t_c, ms	$(Dt_c)^{1/2}/a$	10^6D, cm^2 s^{-1}	d/a
5.3	0.171	2.5	0.0961	5.8	0.178
4.2	0.225	4.2	0.1315	6.4	0.223
3.2	0.315	9.3	0.1907	6.1	0.319
2.9	0.361	11.9	0.2210	6.4	0.358
2.8	0.379	12.4	0.2328	6.8	0.365
2.5	0.446	17.8	0.2768	6.7	0.432

(b) Glass

		t_c, ms		$(Dt_c)^{1/2}/a$		10^6D, cm^2 s^{-1}		d/a	
$i_T/i_{T,\infty}$	d/a	meth 1	meth 2	meth 1	meth 2	meth 1	meth 2	meth 1	meth 2
0.1	0.156	6.9	29.4	0.0829	0.1985	1.6	2.1	0.308	0.266
0.2	0.319	13.8	77.2	0.1730	0.4053	3.4	3.3	0.433	0.419

[a] In the 2nd column d/a is derived from the working curve $i_T(t \to \infty,d)/i_{T,\infty} = f(d/a)$ (*1*), whereas in the last columns it is derived with the working curve $(Dt_c)^{1/2}/a = f(d/a)$ assuming $a = 12.5 \times 10^{-4}$ cm and $D = 6.3 \times 10^{-6}$ cm^2 s^{-1}. $i_T/i_{T,\infty}$ and t_c were measured experimentally.

Note the slope predicted by this equation, $\pi^{-1/2}$ or 0.56, compared to that of the plot in Figure 6, curve A.

Experimental Transients. One can define a procedure for determining t_c, as defined above, for experimental transients and then use the working curves in Figure 6 to determine D or d, independent of any parameter but the tip radius, a, by the following steps. (1) Record the "long distance" transient, and measure the steady-state tip current ($t \to \infty$, $d \to \infty$), $i_{T,\infty}$. (2) Position the tip at a distance d from the substrate, where the steady-state i_T is significantly different from $i_{T,\infty}$. (3) Record the transient $i_T(t,d)$, and normalize it with respect to $i_{T,\infty}$. (4) Evaluate d/a from the steady-state $i_T(t \to \infty,d)/i_{T,\infty}$ and the simulated working curve $i_T(t \to \infty,d)/i_{T,\infty} = f(d/a)$ (*1*). (5) Plot $i_T(t,d)/i_{T,\infty}$ and $i_T(t,d \to \infty)$ versus $t^{-1/2}$, and determine t_c graphically, as shown in Figure 5. (6) Evaluate $(Dt_c)^{1/2}/a$ from d/a and the working curve $(Dt_c)^{1/2}/a = f(d/a)$ (Figure 6), and compute D from the value of $(Dt_c)^{1/2}/a$ read from the working curve and the measured values of t_c and a.

We might point out the similarity of this technique for determining D and the recent method described by Licht et al. (*23*), who used an array of individually addressable microbands to perform a generation–collection experiment and measure the diffusion time between two microbands (a generator and a collector) separated by a known distance. Our approach is similar, since we measure t_c (equivalent to a diffusion time) as a function of the tip–substrate distance, but over a range of distances.

It is important to point out that our technique does not require knowledge of the absolute tip to substrate distance, d. This is an advantage, since it can be experimentally difficult to evaluate an accurate absolute value of d from relative movements of the piezos. The only parameter that needs to be known with precision a priori, is a. We should emphasize that, contrary to most electrochemical techniques, in the SECM transient method the determination of D is independent of the concentration, C^*, and the number of electrons involved during the electrochemical reaction, n. Note that, in principle, it is possible to evaluate t_c for an insulating, as well as a conducting, substrate. For example, with an insulating substrate, it is not necessary for the tip-generated species to be stable, as is required by generation–collection methods. We should stress, however, that the evaluation of D with an insulating substrate will generally not be very precise, since the negative feedback tip current under these conditions (hindered diffusion) is very dependent on the actual geometry of the tip and the substrate (the simulation is based on the assumption that the substrate and tip are perfectly parallel to one another). Because the positive feedback tip current is much less geometry dependent and larger values of $i_T/i_{T,\infty}$ are measured, the evaluation of D with a conducting substrate is more precise.

Two other applications derive from this approach: one can compute C^* from D, a, $i_{T,\infty}$, and n (if n is known) or compute n from D, a, $i_{T,\infty}$, and C^* (if C^* is known). In the former, the bulk concentration is evaluated without the need of a calibration curve, whereas in the latter, the number of electrons can be evaluated for the electrode reaction of a species whose diffusion coefficient is not known a priori.

To demonstrate the approach discussed above, experimental SECM transients were recorded for different tip–substrate distances above a conductor (gold) and an insulator (glass). In actual transients the measured current also contains a contribution from double-layer (dl) charging that depends upon the dl capacitance of the tip and the uncompensated resistance (R_u). Moreover, in general, the potential drops at the tip and biased substrate surfaces can be affected by the magnitude of iR_u, although in the cases considered here the applied bias is sufficiently extreme as to ensure diffusion control. As in most studies involving ultramicroelectrodes (*24*), dl charging and iR_u effects tend to be small, e.g., as compared with analogous experiments in thin-layer cells. The electrochemical reaction occurring on the tip was the oxidation of $Fe(CN)_6^{4-}$ (50 mM bulk concentration) to $Fe(CN)_6^{3-}$ in 1 M KCl. Experimental normalized tip currents are plotted as a function of time (Figure 7) and as a function of the inverse square root of time (Figure 8). For these transients, about 1000 tip current values were recorded at a sampling rate of one point every 100 μs. As expected from the simulation, these results show that a very rapid steady state is established when the tip is close to a conductor (as early as 10 ms, top curve of Figure 7), whereas a quasi steady state occurs when the tip is close to an insulator (a true steady state does not appear on the time scale of these experiments). Since it was difficult to observe true MD behavior at very short times (either because of the double-layer charging current or because of the finite rise time of the current follower), the short time line used to determine t_c, as shown in Figure 5, was obtained from the current transient recorded when the tip was far from the substrate. Plotted as a function of the inverse square root of time, the experimental microdisk transient is a straight line that can be used for the determination of the experimental critical time.

Table IIa shows the results with a gold substrate; $i_T/i_{T,\infty}$ and t_c were experimentally measured. In the second column d/a is computed from the steady-state working curve $i_T(t \to$

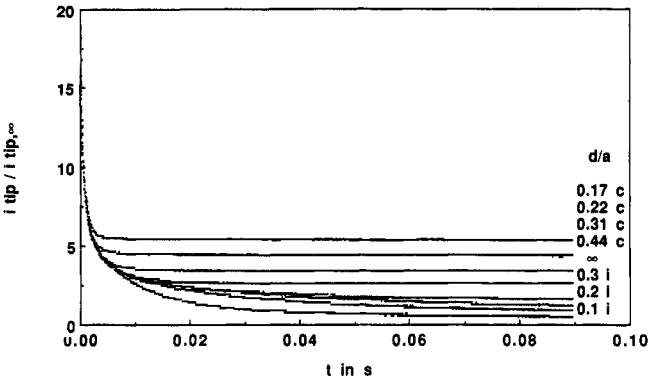

Figure 7. Experimental tip current transients plotted as a function of time. From top to bottom d/a equals 0.17, 0.22, 0.31, and 0.44 above a gold substrate, ∞, and 0.3, 0.2, and 0.1 above a glass substrate.

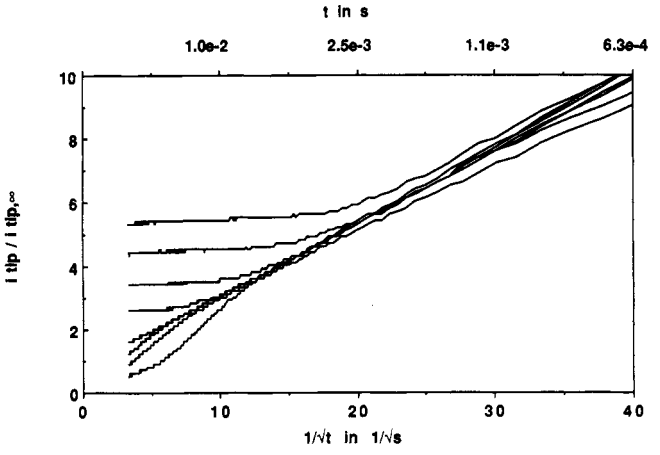

Figure 8. Same experimental transients as in Figure 7, plotted as a function of the inverse square root of time.

$\infty,d)/i_{T,\infty} = f(d/a)$ (*1*), while in the last column d/a is computed with the transient working curve $(Dt_c)^{1/2}/a = f(d/a)$ taking $a = 12.5 \times 10^{-4}$ cm and $D = 6.3 \times 10^{-6}$ cm^2 s^{-1}. (For a 4 mM solution of $K_4Fe(CN)_6$ in 1 M KCl, Adams (*25*) reports a value of 0.632×10^{-5} cm^2 s^{-1} for the diffusion coefficient of $Fe(CN)_6^{4-}$.) Note that both methods lead to almost identical results. Column 5 lists the value of D calculated for each distance; the average is $(6.4 \pm 0.3) \times 10^{-6}$ cm^2 s^{-1}.

Table IIb reports the results with a glass substrate. In this case we compare the two methods for the determination of t_c (method 1 is based on the tangent to the steepest region of the SECM transient; method 2 is based on the intercept of $i_T/i_{T,\infty} = 1$ and the SECM transient). The results for an insulating substrate are much less precise and accurate and are dramatically dependent on the geometry of the tip–substrate system. The microdisk used throughout had an RG (insulating sheath radius/microdisk radius) of about 24, while all of the SECM simulations were performed for an RG of 10.

CONCLUSIONS

The chronoamperometric response of the SECM tip has been studied. An approximate analytical treatment had been proposed. Equations for the chronoamperometric response of a planar electrode, a microdisk, and a thin-layer cell have been used to predict the semiquantitative time dependence of the SECM tip current at very short, intermediate, and long times. The results of a more exact treatment based on a two-dimensional digital simulation of the diffusion process between the tip and the substrate have been presented, and the simulated SECM transients were compared with those predicted by the approximate analytical approach. An analysis of the normalized tip current plotted against the inverse square root of time has led to the measurement of the time when the diffusing species probes the presence and nature of the substrate. A working curve for the tip–substrate distance dependence of this critical time has been reported; it was proposed that this curve be used for the determination of the diffusion coefficient. Experimental SECM transients have been presented and analyzed; a measure of the critical time for several distances above a conducting substrate has shown that this technique allows determination of a value of the diffusion coefficient that agrees with previously published data. However, measurements above an insulating substrate have shown that the tip current is dramatically dependent on the geometry of the tip–substrate system.

ACKNOWLEDGMENT

We thank the University of Texas System Center for High Performance Computing for providing the necessary computing resources. This is paper number 8 in the SECM series.

LITERATURE CITED

(1) Kwak, J.; Bard, A. J. *Anal. Chem.* **1989**, *61*, 1221.
(2) Bard, A. J.; Fan, F.-R. F.; Kwak, J.; Lev, O. *Anal. Chem.* **1989**, *61*, 132.
(3) Davis, J. M.; Fan, F.-R. F.; Bard, A. J. *J. Electroanal. Chem. Interfacial Electrochem.* **1987**, *238*, 9.
(4) Hüsser, O. E.; Craston, D. H.; Bard, A. J. *J. Electrochem. Soc.* **1989**, *136*, 3222.
(5) Hüsser, O. E.; Craston, D. H.; Bard, A. J. *J. Vac. Sci. Technol. B* **1988**, *6*, 1873.
(6) Mandler, D.; Bard, A. J. *J. Electrochem. Soc.* **1989**, *136*, 3143.
(7) Wuu, Y. M.; Fan, F.-R. F.; Bard, A. J. *J. Electrochem. Soc.* **1989**, *136*, 885.
(8) Mandler, D.; Bard, A. J. *J. Electrochem. Soc.* **1990**, *137*, 1079.
(9) Mandler, D.; Bard, A. J. *J. Electrochem. Soc.* **1990**, *137*, 2468.
(10) Lee, C.; Kwak, J.; Bard, A. J. *Proc. Natl. Acad. Sci. U.S.A.* **1990**, *87*, 1740.
(11) Kwak, J.; Lee, C.; Bard, A. J. *J. Electrochem. Soc.* **1990**, *137*, 1481.
(12) Wipf, D. O.; Bard, A. J. *J. Electrochem. Soc.* **1991**, *138*, 469.
(13) Kwak, J.; Bard, A. J. *Anal. Chem.* **1989**, *61*, 1794.
(14) Bard, A. J.; Faulkner, L. *Electrochemical Methods*; Wiley: New York, 1980.
(15) Shoup, D.; Szabo, A. *J. Electroanal. Chem. Interfacial Electrochem.* **1982**, *140*, 237.
(16) Hubbard, A. T.; Anson, F. C. In *Electroanalytical Chemistry*; Bard, A. J., Ed.; Marcel Dekker: New York, 1970; Vol. 4, p 156.
(17) Oglesby, D. M.; Omang, S. H.; Reilley, C. N. *Anal. Chem.* **1965**, *37*, 1312.
(18) Friedrichs, M. S.; Friesner, R. A.; Bard, A. J. *J. Electroanal. Chem. Interfacial Electrochem.* **1989**, *258*, 243.
(19) Kavanaugh, T. C.; Friedrichs, M. S.; Friesner, R. A.; Bard, A. J. *J. Electroanal. Chem. Interfacial Electrochem.* **1990**, *283*, 1.
(20) Friesner, R. A.; Tuckerman, L. S.; Dornblaser, B. C.; Russo, T. V. *J. Sci. Comput.* **1989**, *4*, 327.
(21) Friesner, R. A.; Tuckerman, L. S.; Dornblaser, B. C. Unpublished work.
(22) Unwin, P. R.; Bard, A. J. Unpublished work.
(23) Licht, S.; Cammarata, V.; Wrighton, M. S. *J. Phys. Chem.* **1990**, *94*, 6233.
(24) Wipf, D. O.; Wightman, R. M. In *Electroanalytical Chemistry*; Bard, A. J., Ed.; Marcel Dekker: New York, 1989; Vol. 15, pp 267–353.
(25) Adams, R. N. *Electrochemistry at Solid Electrodes*; Marcel Dekker: New York, 1969.

RECEIVED for review October 30, 1990. Accepted March 11, 1991. The support of this research by the Texas Advanced Research Program and the National Science Foundation (Grant CHE 8901450) is gratefully acknowledged. B.C.D. gratefully acknowledges the Texas Advanced Research Program and the Robert A. Welch Foundation (Grant F-928). R.A.F. is a Camille and Henry Dreyfus Teacher-Scholar and a recipient of a Research Career Development Award from the NIH, Institute of General Medical Sciences. L.S.T. is supported in part by NSF Grant No. DMS-8901767.